

## Bi-Target Tracking Based on Vortex Wave with Orbital Angular Momentum

Bo Tang<sup>1, \*</sup>, Jian Bai<sup>2</sup>, and Kunyi Guo<sup>3</sup>

**Abstract**—This paper studies the application of vortex wave with orbital angular momentum (OAM) in the radar. The vortex waves can have eigenstates or modes with different integer topological charges, which are orthogonal to each other. The eigenstates with topological charges of 0,  $-1$  and  $1$  were utilized in this paper. The radar transmitted the pulse with topological charge of 0 and received echoes with topological charges of 0,  $-1$  and  $1$ . The receiver can process the signals received by these orthogonal modes to obtain the azimuth and elevation angles of the two targets in a same range gate. Compared with the traditional mono-pulse radar only with sum beam and difference beam, this vortex-wave-based radar can track two targets in principle. This is meaningful for the application of the vortex wave.

### 1. INTRODUCTION

The classical electromagnetic (EM) field theory shows that the EM wave can carry angular momentum [1]. The angular momentum includes the spin angular momentum and orbital angular momentum (OAM) [2]. The spin angular momentum is the polarization for the EM wave. The OAM-carrying beam has the Poynting vector that is not coplanar with the propagation axis. The Laguerre-Gauss vortex beams are the most popular OAM-carrying beams [3]. OAM was studied in the optical field at first [2]. OAM carrying light beam can be used as optical spanners, optical tweezers, and can increase the channel capacity without expanding the bandwidth. Different OAM modes of the light using the same wave band can transmit the signal simultaneously without symbol interruption because of the orthogonality of OAM modes. In 2004, the light beam with OAM was first used in the optical communication [4]. In 2007, the method of utilizing circular array antenna (UCAA) to generate the OAM radio wave was presented in [5]. The UCAA was configured to generate different OAM modes, and the number of eigenstates of the UCAA was discussed in [6]. OAM-carrying radio wave was verified experimentally in 2011 [7]. The wireless communication based on the OAM-carrying radio wave was performed in 2012 [8]. In recent years, the OAM in microwave band has been a hotspot of the research. Because the vortex wave with orthogonal OAM eigenstates can make independent wireless channels for the mobile communication, this has been considered as an alternative way to overcome the limitation of the spectrum resources. So, many researches have been made on how to generate the vortex wave and test it and how to use it in the wireless communication in microwave band. In [7, 8], a modified parabolic dish antenna and a spiral reflector were used to generate OAM respectively. In [9], a circular time-switched array (TSA) was studied, which is similar to UCAA, but only one element was energized in one moment. And a modified UCAA was given in [10] by locating the elements on a helix. The OAM-carrying radio wave in 10 GHz band was generated based on a circular phased array [11]. In [12], OAM

---

*Received 6 March 2017, Accepted 10 May 2017, Scheduled 26 May 2017*

\* Corresponding author: Bo Tang (tangbohr@hotmail.com).

<sup>1</sup> School of Computer and Communication Engineering, University of Science and Technology Beijing, Beijing 100083, China. <sup>2</sup> Science and Technology on Millimeter-wave Laboratory, Second Research Institute of the China Aerospace Science and Industry Group, Beijing 100039, China. <sup>3</sup> Center for Electromagnetic Simulation, School of Information and Electronics, Beijing Institute of Technology, Beijing 100081, China.

was applied in the millimeter communication for multiplexing. In [13], it was demonstrated that OAM radio transmission and MIMO wireless system have the equal available channel capacity for certain array configurations in free space. Besides the application in the wireless communication, OAM radio wave can also be used in the radar research field. For example, [14] studied the imaging method based on the OAM radio wave. Because the wave front of the OAM radio wave is vortex, the target detecting with radar will be special compared with the plane wave. So it is significant to study the application of the OAM radio wave in radar.

Based on the analysis of the characteristics of the OAM radio wave and mono-pulse radar, this paper applies the OAM radio wave with topological charges 0,  $-1$  and  $1$  to the mono-pulse radar. Note that OAM radio wave with topological charges 0 is a plane wave, which is considered as a special vortex wave here.

## 2. THE OAM-CARRYING VORTEX WAVE GENERATED BY UCAA

The OAM-carrying wave can be generated by a parabolic dish antenna, spiral reflector, perforated dielectrics lens antenna, and UCAA [5–10]. For convenience and without loss of generality in principle, the following analysis is based on UCAA method to generate OAM radio wave [8]. The uniform circular antenna array is shown in Fig. 1. There are  $N$  antennas located in a circular baseline. All the antennas have the same shapes and orientations. The spherical coordinates system is set in Fig. 1. The circle is in  $\theta = \pi/2$  plane ( $XY$  plane), and the center of the circular is the origin of the coordinates system. The normal line of the circular is along the  $Z$  axis.

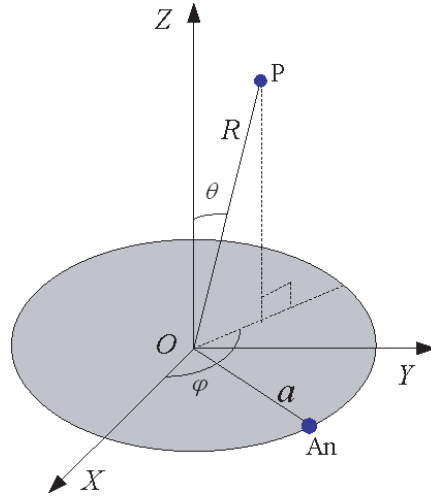


**Figure 1.** The coordinates system.

In spherical coordinates, point P is located in  $(R, \theta, \varphi)$ , and the  $n$ th antenna is located in  $(a, \pi/2, \varphi_{a,n})$ .  $\theta$  is the angular value in the elevation in spherical coordinates at point P;  $\varphi$  and  $\varphi_{a,n}$  are azimuth angular values in spherical coordinates for point P and the  $n$ th antenna, respectively.  $a$  is the radius of the circle. Each antenna has a uniform pattern. The original phase of the  $n$ th antenna is  $\psi_n = ln\frac{2\pi}{N}$ , where  $l$  is the mode number,  $l = 0, \pm 1, \pm 2, \dots$ . The distance between P and the  $n$ th antenna is

$$R_n = \sqrt{R^2 + a^2 - 2Ra \sin \theta \cos(\varphi - \varphi_{a,n})} \quad (1)$$

If P is located in the far zone of the radiation, then the electric field on P can be expressed as [14]

$$\begin{aligned} E &= A \sum_{n=1}^N \frac{1}{R_n} \exp(-jkR_n) \exp(jl\Delta\psi) \\ &\approx Aj^l \frac{N}{R} \exp(-jkR) \exp(jl\varphi) J_l(ka \sin \theta) \end{aligned} \quad (2)$$

where  $A$  is a constant;  $k$  is the wave number;  $\Delta\psi = 2\pi n/N = \varphi_{a,n}$ ;  $R$  is the distance between P and the original point;  $J_l$  is the  $l$ th order Bessel function of the first kind. When  $l = 0$ , it is denoted that

$$m_0(\theta) = A \frac{N}{R} \exp(-jkR) J_0(ka \sin \theta) \tag{3}$$

where  $J_0$  is the zeroth order Bessel function of the first kind. When  $l = 1, -1$ , it is denoted that

$$m_1(\theta, \varphi) = jA \frac{N}{R} \exp(-jkR) \exp(j\varphi) J_1(ka \sin \theta) \tag{4}$$

$$m_{-1}(\theta, \varphi) = -jA \frac{N}{R} \exp(-jkR) \exp(-j\varphi) J_{-1}(ka \sin \theta) \tag{5}$$

where  $J_1$  and  $J_{-1}$  are the first order and the negative first order Bessel functions of the first kind, respectively. The term  $\exp(\pm j\varphi)$  shows that the wave vector of the front plane of the wave has the component in the azimuth, which means that it is a vortex wave. The term  $J_{\pm 1}(ka \sin \theta)$  indicates that it is zero in the radial axis.

### 3. THE PRINCIPLE OF THE BI-TARGET TRACKING BASED ON VORTEX WAVE

The vortex wave based radar transmits the pulse with the mode of  $l = 0$  and receives the echoes with three modes of  $l = 0, l = -1$  and  $l = 1$ . It is shown in Fig. 2.

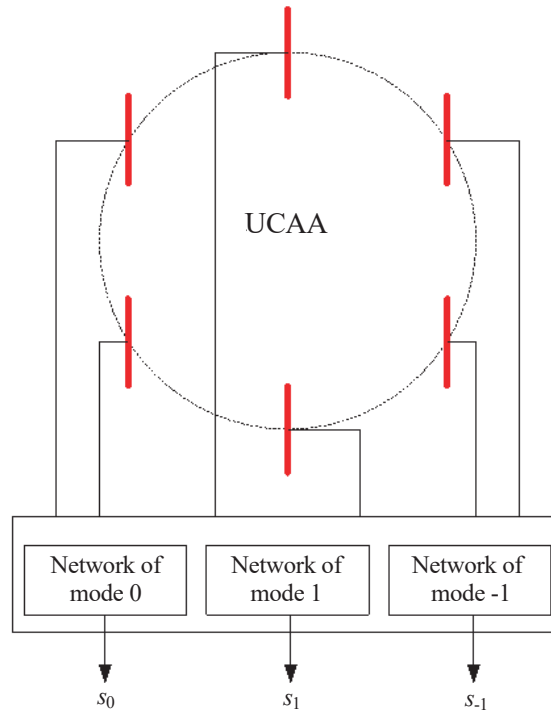


**Figure 2.** Scheme of UCAA structure with three receiving modes.

The received echoes can be described as

$$s_0(\theta_1, \theta_2) = m_0(\theta_1) \delta_1 + m_0(\theta_2) \delta_2 \tag{6}$$

$$s_1(\theta_1, \varphi_1, \theta_2, \varphi_2) = m_1(\theta_1) \delta_1 + m_1(\theta_2) \delta_2 \tag{7}$$

$$s_{-1}(\theta_1, \varphi_1, \theta_2, \varphi_2) = m_{-1}(\theta_1) \delta_1 + m_{-1}(\theta_2) \delta_2 \tag{8}$$

where  $\delta_1$  and  $\delta_2$  are factors of the targets' scattering characteristics. The received echoes can give the ratio  $\gamma_1$  and  $\gamma_{-1}$  based on these modes. If the noise is ignored, and the ratios  $\gamma_1$  and  $\gamma_{-1}$  can be given

as the following.

$$\gamma_1(\theta_1, \theta_2, \varphi_1, \varphi_2) = \frac{s_1}{s_0} = j \frac{J_1(ka \sin \theta_1) \exp(j\varphi_1) \delta_1 + J_1(ka \sin \theta_2) \exp(j\varphi_2) \delta_2}{J_0(ka \sin \theta_1) \delta_1 + J_0(ka \sin \theta_2) \delta_2} \quad (9)$$

$$\gamma_{-1}(\theta_1, \theta_2, \varphi_1, \varphi_2) = \frac{s_{-1}}{s_0} = -j \frac{J_{-1}(ka \sin \theta_1) \exp(-j\varphi_1) \delta_1 + J_{-1}(ka \sin \theta_2) \exp(-j\varphi_2) \delta_2}{J_0(ka \sin \theta_1) \delta_1 + J_0(ka \sin \theta_2) \delta_2} \quad (10)$$

When  $ka \sin \theta_1, ka \sin \theta_2 \ll 1$ , it can be obtained that

$$\gamma_1(\theta_1, \theta_2, \varphi_1, \varphi_2) = j \frac{1}{2} ka \frac{\theta_1 \exp(j\varphi_1) \delta_1 + \theta_2 \exp(j\varphi_2) \delta_2}{\delta_1 + \delta_2} \quad (11)$$

$$\gamma_{-1}(\theta_1, \theta_2, \varphi_1, \varphi_2) = j \frac{1}{2} ka \frac{\theta_1 \exp(-j\varphi_1) \delta_1 + \theta_2 \exp(-j\varphi_2) \delta_2}{\delta_1 + \delta_2} \quad (12)$$

When there are two targets, that is  $\delta_1, \delta_2 \neq 0$ , it can be derived from Eqs. (11)–(12) that

$$\theta_1 \exp(j\varphi_1) = \Lambda_1 \quad (13)$$

$$\theta_2 \exp(j\varphi_2) = \Lambda_2 \quad (14)$$

where

$$\Lambda_1 = \frac{\gamma_{-1} \cdot (\delta_1 + \delta_2) \delta_2^* + \gamma_1^* \cdot (\delta_1^* + \delta_2^*) \delta_2}{j \frac{1}{2} ka (\delta_1 \delta_2^* - \delta_2 \delta_1^*)} \quad (15)$$

$$\Lambda_2 = \frac{\gamma_1 \cdot (\delta_1 + \delta_2) \delta_1^* + \gamma_{-1}^* \cdot (\delta_1^* + \delta_2^*) \delta_1}{j \frac{1}{2} ka (\delta_2 \delta_1^* - \delta_1 \delta_2^*)} \quad (16)$$

where the superscript of asterisk means complex conjugate of the counterpart. Then, the coordinates  $(\theta_1, \varphi_1)$  and  $(\theta_2, \varphi_2)$  of the two targets can be obtained.

Compared with that the traditional mono-pulse radar has difficulties to track two targets simultaneously, this vortex wave method with topological charges 0,  $-1$  and  $1$  ( $l = 0, -1, 1$ ) can track two targets in a same range gate.

When there is only one target, that is  $\delta_1 \neq 0, \delta_2 = 0$ , the result of  $(\theta_1, \varphi_1)$  can be obtained from Eqs. (11)–(12) as that

$$\varphi_1 = \arg \gamma_1 - \frac{\pi}{2} \quad (17)$$

$$\theta_1 = 2 \frac{|\gamma_1|}{ka} \quad (18)$$

On this mono-target case, the signal processing of the mono-pulse radar is based on the spherical coordinates. In fact, the vortex wave can be regarded as a special method of the signal processing as indicated in [13].

The values of  $\delta_1$  and  $\delta_2$  are needed for the solution of Eqs. (15), (16).  $\delta_1$  and  $\delta_2$  can be obtained by the method similar to mobile-target-detection (MTD) method based on the pulse string [15]. When  $ka \sin \theta_1, ka \sin \theta_2 \ll 1$ , it can be obtained from Eq. (6) that

$$s_0 = A \frac{N}{R} e^{-jkR} [J_0(ka \sin \theta_1) \delta_1 + J_0(ka \sin \theta_2) \delta_2] \cong A \frac{N}{R} e^{-jkR} (\delta_1 + \delta_2) \quad (19)$$

Then, the value of  $|\delta_1 + \delta_2|^2$  can be obtained.

$$|\delta_1 + \delta_2|^2 = p \quad (20)$$

$$p = \frac{|s_0|^2 R^2}{|A|^2 N^2} \quad (21)$$

That is,

$$|\delta_1|^2 + |\delta_2|^2 + 2|\delta_1 \delta_2| \cos(\varphi_{\delta_1} - \varphi_{\delta_2}) = p \quad (22)$$

where  $\varphi_{\delta_1}, \varphi_{\delta_2}$  are the phases of  $\delta_1$  and  $\delta_2$ , respectively. If the radial component of the velocity difference of the two targets is  $\Delta v$ , then

$$\varphi_{\delta_1} - \varphi_{\delta_2} = k \Delta v \cdot t = h \cdot k \Delta v \cdot \Delta t + \alpha \quad (23)$$

where  $\Delta t$  is the pulse-repetition period, and  $\alpha$  is the initial phase difference. One value of  $|\delta_1 + \delta_2|^2$  will be obtained through one pulse transmitting. So,

$$|\delta_1|^2 + |\delta_2|^2 + 2|\delta_1\delta_2| \cos(h \cdot k\Delta v \cdot \Delta t + \alpha) = p(h) \tag{24}$$

where  $h$  is the number of the transmitted pulses. Taking the Fourier transformation of the data series of  $p(h)$ , there will be three peak values in the frequency domain. The peak values are located on  $0, \pm k\Delta v$ . The initial phase  $\alpha$  can also be obtained by the phase of the peak value. Therefore, the values of  $\Delta v$  and  $\alpha$  can be obtained. Then,  $\varphi_{\delta_1} - \varphi_{\delta_2}$  can be obtained. Consequently,  $|\delta_1|$  and  $|\delta_2|$  can be obtained based on Eq. (24).

#### 4. NUMERICAL RESULTS

The above analysis is based on the approximation for  $ka \sin \theta_1, ka \sin \theta_2 \ll 1$ . So, the numerical simulation needs to be performed to validate the above analysis. The factors used in the calculation are as follows. When  $t = 0$ , in  $XYZ$  coordinates system, the coordinates of the two targets are  $X_1 = Y_1 = 0, X_2 = Y_2 = 0, Z_1 = Z_2 = 10000$  m. The radar is located on the original point. The velocity of target one is 300 m/s, and the velocity of target two is 310 m/s; the direction of the velocity of target one is aligned to  $\varphi = \pi/4$  in  $Z = 10000$  m plane, and direction of the velocity of target two is aligned to  $\varphi = 2\pi/9$  in  $Z = 10000$  m plane. The radar working frequency is 15 GHz, and the radius of UCAA is 0.1 m.  $|\delta_1| = |\delta_2| = 1$ . The phase difference between  $\delta_1$  and  $\delta_2$  is determined through the Fourier transformation of the echoes of the pulse string. The direction of the radar beam is toward the position where target one located just 1 ms ago. The beam footprint of radar is shown in Fig. 3. The solid point is the position of the targets at that time.

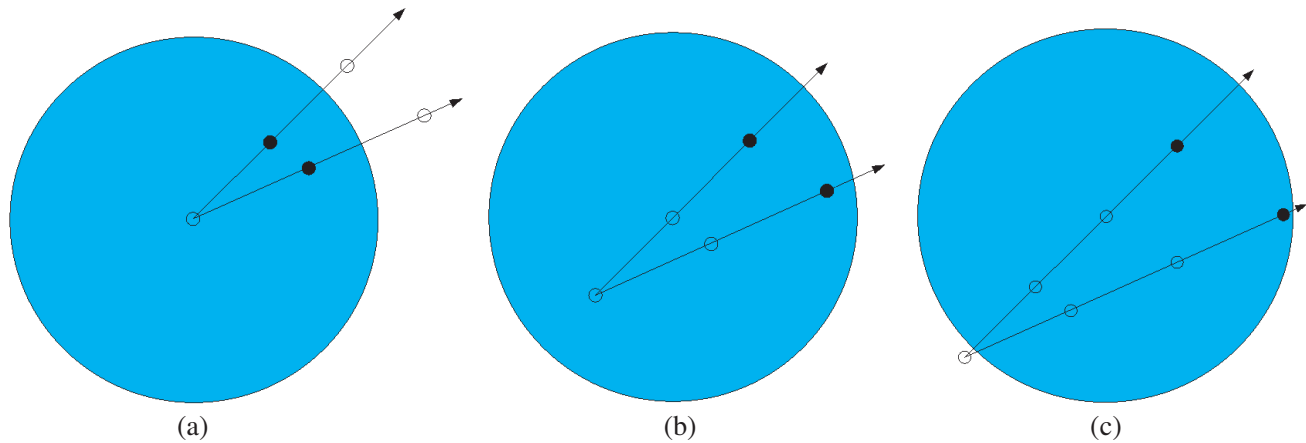


**Figure 3.** The beam footprint of radar for two targets. (a) 0 ms. (b) 1 ms. (c) 2 ms.

In Figs. 4–7, the horizontal ordinate is time which is from 0–1000 ms, the vertical ordinate is  $X$  or  $Y$  coordinates of the targets in meters. In Fig. 4 and Fig. 5, the numerical results are based on Eqs. (9)–(10). In Fig. 6 and Fig. 7, the numerical results are based on Eqs. (9)–(10) with additional noise to the numerator and denominator in Eqs. (9)–(10). Matlab is used for computation. The Bessel function is generated by the Matlab function of `Besselj()`. The additional Gaussian noise is generated by `randn()` function.

In Fig. 4 and Fig. 5, the real location of the target is depicted as the dashed line in  $X$  and  $Y$  coordinates, respectively, and the estimated location of the target is depicted as the solid line. It can be seen from Fig. 4 and Fig. 5 that the estimated location is agreeable to the real location. There are some vibrations due to the approximation for  $ka \sin \theta_1, ka \sin \theta_2 \ll 1$ .

On the condition that there is  $-40$  dB additional Gaussian white noise in the received signal, the real location of the target is depicted in Fig. 6 and Fig. 7 as the dashed line in  $X$  and  $Y$  coordinates, respectively, and the estimated location of the target is depicted as the solid line in Fig. 6 and Fig. 7.

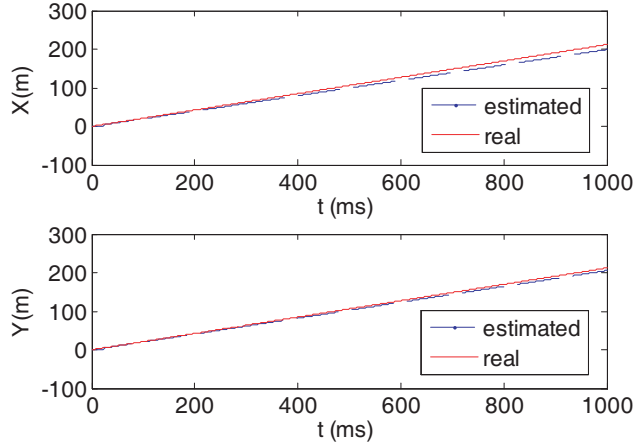


**Figure 4.** The location of target one.

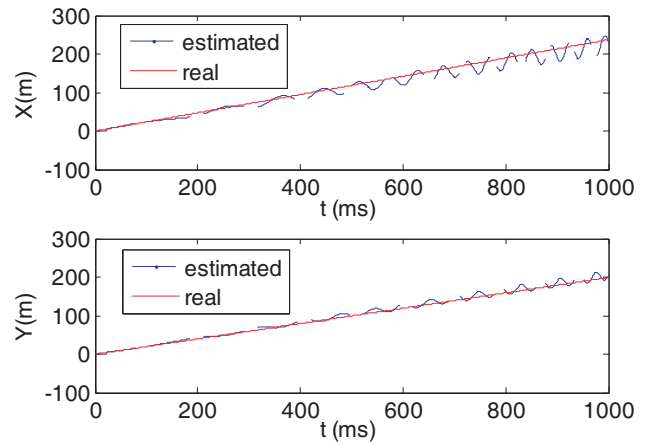


**Figure 5.** The location of target two.

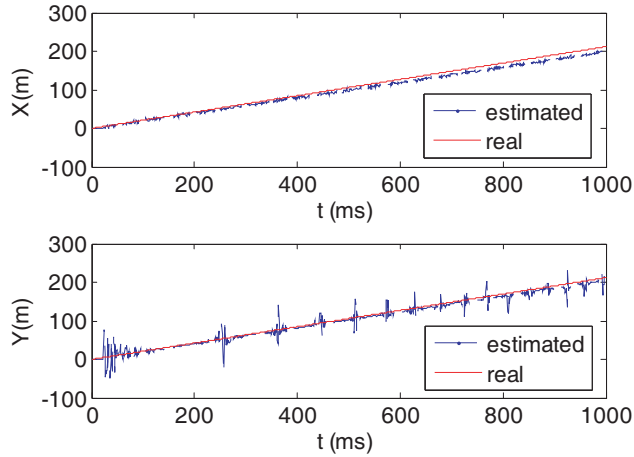


**Figure 6.** The location of target one (with noise).

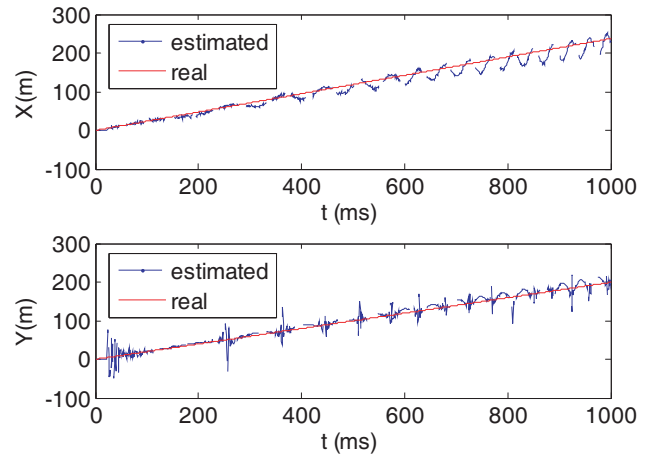


**Figure 7.** The location of target two (with noise).

It can be seen that the estimated location is still agreeable to the real location. Although there are occasional deviations on the line, it can be dealt with through radar signal processing.

## 5. CONCLUSIONS

This paper gives a method to track two targets simultaneously by using the transmitting beam and the receiving beams based on the vortex wave. The vortex wave can carry OAM with different beam orthogonal modes. The radar transmits the pulse with the zeroth mode and receives the echoes with multiple modes. Based on the three receiving modes with topological charges of 0, 1 and  $-1$ , respectively, the locations of the two targets can be obtained by the received signals from the three modes of vortex wave. The analysis is validated by the numerical results. The numerical results show that the estimated location of the targets is very close to the real location of the targets. Therefore, the vortex wave with multiple modes has the potential ability to help the mono-pulse radar track two targets simultaneously. This is the vortex wave's possible application in the radar.

## ACKNOWLEDGMENT

This work is supported by the National Natural Science Foundation of China (Grant No. 61471041) and the Fundamental Research Funds for the Central Universities (FRF-TP-15-028A3).

## REFERENCES

1. Jackson, J. D., *Classical Electrodynamics*, 24–47, Wiley, New York, 1962.
2. Allen, L., M. W. Beijersbergen, R. J. C. Spreeuw, et al., “Orbital angular momentum of light and the transformation of Laguerre-Gaussian modes,” *Phys. Rev. A*, Vol. 45, No. 11, 8185–8189, 1992.
3. Someda, C. G., *Electromagnetic Waves*, 2nd edition, Sec. 5.6, CRC Press, Boca Raton, FL, USA, 2006.
4. Gibson, G., J. Courtial, M. J. Padgett, et al., “Free-space information transfer using light beams carrying orbital angular momentum,” *Opt. Express*, Vol. 12, No. 22, 5448–5456, 2004.
5. Thide, B., H. Then, J. Sjöholm, et al., “Utilization of photon orbital angular momentum in the low-frequency radio domain,” *Physical Review Letters*, 2007, Vol. 99, No. 8, 087701-1–087701-4.
6. Mohammadi, S. M., L. K. S. Daldorff, J. E. S. Bergman, et al., “Orbital angular momentum in radio — A system study,” *IEEE Trans. Ant. Propag.*, Vol. 58, 565–572, 2010.
7. Tamburini, F., E. Mari, B. Thide, C. Barbieri, and F. Romanato, “Experimental verification of photon angular momentum and vorticity with radio techniques,” *Appl. Phys. Lett.*, Vol. 99, No. 20, 321, 2011.
8. Tamburini, F., E. Mari, A. Sponselli, F. Romanato, and T. Bo, “Encoding many channels in the same frequency through radio vorticity: First experimental test,” *New Journal of Physics*, Vol. 3, 033001, 2012.
9. Tennant, A. and B. Allen, “Generation of OAM radio waves using circular time-switched array antenna,” *Electron. Lett.*, Vol. 48, No. 2, 1365–1366, 2012.
10. Yuan, T., Y. Cheng, H. Wang, et al., “Generation of OAM radio beams with modified uniform circular array antenna,” *Electronics Letters*, Vol. 52, No. 11, 896–898, 2016.
11. Bai, Q., A. Tennant, and B. Allen, “Experimental circular phased array for generating OAM radial beams,” *Electron. Lett.*, Vol. 50, No. 20, 1414–1415, 2014.
12. Yan, Y., et al., “High-capacity millimetre-wave communications with orbital angular momentum multiplexing,” *Nature Comm.*, Vol. 5, 4876, 2014.
13. Edfors, O. and A. J. Johansson, “Is orbital angular momentum (OAM) based radiocommunication an unexploited area?” *IEEE Trans. Ant. Propag.*, Vol. 60, No. 2, 1126–1131, 2012.
14. Liu, K., Y. Cheng, Z. Yang, and H. Wang, “Orbital-angular-momentum-based electromagnetic vortex imaging,” *IEEE Antennas & Wireless Propagation Letters*, Vol. 14, 711–714, 2015.
15. Skolnik, M. I., *Radar Handbook*, 3rd edition, Sec. 2.2, McGraw-Hill, New York, 2008.